IJES *Iranian Journal of Earth Sciences*
Vol. 11, No. 4, 2019, 267-276.

Inverse modeling of gravity field data due to finite vertical cylinder using modular neural network and least-squares standard deviation method

Ata Eshaghzadeh*[1]; Sanaz Seyedi Sahebari[2]; Roghayeh Alsadat Kalantari[1]

1. Postgraduate of Geophysics, Zima Company, Chalus, Iran
2. Roshdiyeh Higher Education Institute, Tabriz, Iran

Received 26 January 2018; accepted 3 November 2018

Abstract

In this paper, modular neural network (MNN) inversion has been applied for the parameters approximation of the gravity anomaly causative target. The trained neural network is used for estimating the amplitude coefficient and depths to the top and bottom of a finite vertical cylinder source. The results of the applied neural network method are compared with the results of the least-squares standard deviation method. The inverse modeling has been tested first on synthetic gravity data. The synthetic data are infected with random noise to evaluate the effect of noise on performance of the methods. Both methods show satisfactory results, with and without random noise. The MNN and least squares standard deviation approaches have been applied to two real gravity data due to two salt domes from Iran and USA, where the results comparison shows good agreement with each other. The computed standard errors indicate the generated gravity response of the estimated parameters from MNN has better conformity with the observed gravity anomaly than the generated gravity response from the least squares method. The results of the MNN inversion show the top and bottom depths of the salt dome situated in Iran are about 24.5 m and 63.8 m and for the salt dome situated in USA are about 1451 m and 9263 m, respectively.

Keywords: *Salt Dome, Finite Vertical Cylinder, Least-Squares Standard Deviation, Modular Neural Network (MNN)*

1. Introduction

To consider a simple geometrically shaped model for buried structures can be very useful in quantitative analysis of gravity data, as ambiguity in interpretation reduce dramatically. One of the most important exploration problems is estimating the shape and depth of an anomaly causative mass. Different methods have been developed to determine the shape and depth of the buried structure from gravity data.

The methods generally fall into one of two categories. The first category is the continual modeling methods, such as Talwani and Ewing (1960), Tanner (1967) and Cordell and Henderson (1968). However, the methods require information about density and depth as part of the input data obtained from geological studies and/or other geophysical methods. Thus, the resulting model based on these parameters can change infinitely. The second category is the graphical methods, such as Masket et al. (l956), Skeels (1963), Botezatu et al. (1971) and Pick et al. (l973). Moreover, some people illustrated that the window curves method can be employed to compute the depth and shape of the buried mass from gravity data (Abdelrahman and El-Arabi 1996; Abdelrahman et al. 2001; Essa 2007). Abdelrahman et al. (2006) expanded a least-squares variance analysis method for shape and depth estimation from gravity field data.

*Corresponding author.
E-mail address (es): eshaghzadeh.ata@gmail.com

Nowadays Artificial Neural Networks (ANNs) are of main research concern, so that involving researchers of various disciplines and sciences. Topics contributing to this investigation contain biology, computing, electronics, mathematics, medicine, geophysics and etc (Bichsel 2005). The new method, the artificial neural network, has been employed in recent years for different branch of geophysics especially potential fields. For example, the situation of buried steel drums as magnetic dipole source is evaluated using supervised artificial neural network (Salem et al. 2001). Eslam et al. (2001) specified depth and radius of subsurface cavities from microgravity data using back propagation neural networks. Hajian (2004) estimated depth and shape factor of the gravity anomaly source by applying Feed-Forward Back-Propagation Neural Networks. Chua and Yang (1998) defined a new approach in neural networks titled Cellular Neural Network (CNN), which is focused on 2D image processing. CNN was applied for separation of regional/residual potential sources in geophysics (Albora et al. 2001a, 2001b). Forced Neural Networks for gravity anomaly analysis was proposed by Osman et al. (2006, 2007). Abedi et al. (2009) calculated the depth and radius of the simple geometry by the neural network from the gravity anomalies. Al-Garni (2013) used MNN inversion for estimating the depth of the gravity anomaly source related to simple geometry such as sphere, infinite horizontal cylinder and semi-infinite vertical cylinder. Eshaghzadeh and Kalantari (2015) have been proposed a new method

based on feed-forward neural network for gravity field inverse modeling due to anticlinal structures. Eshaghzadeh and Hajian (2018) have introduced a new concept of the modularity for analysis the gravity field by modular neural network.

In this paper, first Abdelrahman and Abo-Ezz (2008) method is applied to determine the depth to the top and base of a buried finite vertical cylinder from moving average residual anomaly profiles obtained numerically from gravity data using filters of successive window lengths. The standard deviation of the depths to the top can be investigated as a criterion for determining the correct top and base depth of the subsurface structure. Afterward, the modular neural network is used for inverse modeling of profile gravity data. We investigate the ability of the suggested approach in estimating the radius and the depth to the top and bottom of buried finite vertical cylinder structure from calculated gravity data, with and without random noise. The MNN inversion and least-squares standard deviation method are employed for analysis of a real gravity data set of two salt domes from Iran and USA.

2. Least-squares standard deviation method

The gravity effect of a finite vertical cylinder is defined by Hammer (1974)

$$g(\mathrm{x}) = KF(\mathrm{x}) \tag{1}$$

Where k is amplitude coefficient as

$$F(x_i) = \frac{1}{\sqrt{x^2+z^2}} - \frac{1}{\sqrt{x^2+h^2}}, \quad \mathrm{K} = \pi \mathrm{G}\rho \mathrm{R}^2$$

where x is the horizontal location coordinate of measurement points, z and h represent the depths to the top and base planes of causative structure from ground surface respectively, G is the gravitational constant, R is the radius of the horizontal cross section of a vertical cylinder, and ρ is the density contrast (Fig 1).

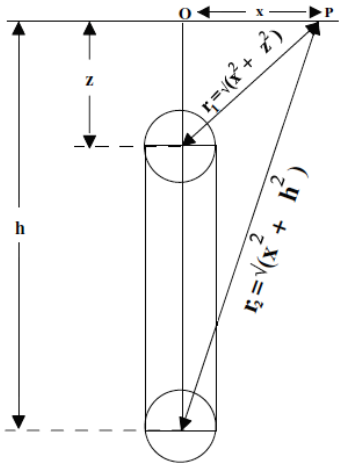

Fig 1. Geometries of the finite vertical cylinder

Three observation points x_i-s, x_i and $x_i + s$ are considered on the residual gravity anomaly profile where $s = 1,\ldots, M$ interval units and is named the window length. The moving average residual gravity anomaly $g_r(x_i)$ at the observation point x_i was given by Abdelrahman and Abo-Ezz (2008) in the following form:

$$g_r(x_i) = \frac{K}{2}\left[2F(x_i) - F(x_i + s) - F(x_i - \mathrm{s})\right], \ldots i = 1,2,3,\ldots,N. \tag{2}$$

$g_r\ (xi)$ achieves its most extreme at $x_i = 0$, which is computed by

$$g_r(\max) = KE(h,z) \tag{3}$$

Where $E(h,z) = \frac{h-z}{zh} - \frac{1}{\sqrt{s^2+z^2}} + \frac{1}{\sqrt{s^2+h^2}}$

Equation (2) can now be rewritten as (Abdelrahman and Abo-Ezz 2008)

$$g_r(x_i) = \frac{g_r(\max)}{2} D(\mathrm{x}_i) \tag{4}$$

Where $D(x_i) = \left(\frac{2F(x_i) - F(x_i + s) - F(x_i - \mathrm{s})}{E(z,h)}\right)$

The unknown top depth (z) of the structure in equation (4) can be attained by minimizing, i.e.

$$\lambda(z) = \sum_{i=1}^{N}\left[H(\mathrm{x}_i) - \frac{g_r(\max)}{2} D(\mathrm{x}_i)\right]^2 = \min, \tag{5}$$

where $H(x_i)$ signifies the observed moving average residual gravity anomalies at x_i.

Setting the derivative of $\lambda(z)$ to zero as for z lead-in to (Abdelrahman and Abo-Ezz 2008)

$$u(z) = \sum_{i=1}^{N}\left[H(\mathrm{x}_i) - \frac{g_r(\max)}{2} D(\mathrm{x}_i)\right] D^*(\mathrm{x}_i) = 0, \tag{6}$$

Where

$$D^*(\mathrm{x}_i) = \frac{\partial D(\mathrm{x}_i)}{\partial z}$$

Nonlinear equation (6) can be worked out for z using standard methods such as Newton–Raphson method as the depth to the bottom (h) remains unchangeable during the solving process. Thus, the depth to the top is estimated by solving one nonlinear equation in z.

Theoretically, one value of the window length, i.e. s, is enough to compute the depth to the top from equation (6), but in practice, more than one value of the window length is used because of the presence of noise in data set and interference from neighboring sources. In this method, criterion for determining the exact depth to the top and base of the causative structure is the minimum standard deviation (Abdelrahman and Abo-Ezz 2008). The lowest standard deviation indicates the best value of the assumed depth to the base and the correct values for computed depth to the top based on the different windows length.

2.1. Synthetic example

We have considered a finite vertical cylinder model with K=-20 mGal.m ,z=10 m and h=30 m. Moreover, for evaluating the stability of the least squares method, random errors of 5% were added to synthetic gravity data. Four successive moving average windows are employed to each set of input data, that is, the free-noise and noise corrupted synthetic gravity data (Figs. 2 and 3).

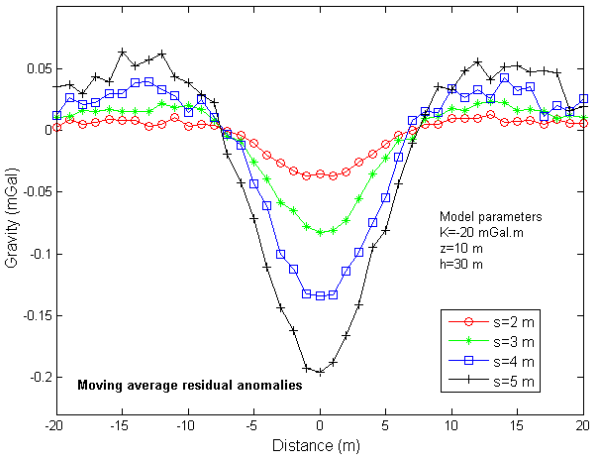

Fig 2. Moving average residual gravity anomalies due to a buried finite vertical cylinder model for s = 2, 3, 4, and 5 m.

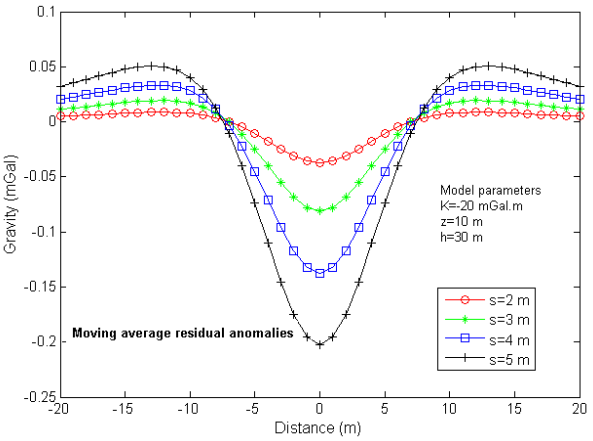

Fig 3. Moving average residual gravity anomalies due to a buried finite vertical cylinder model for s = 2, 3, 4, and 5 m after adding 5% of random noise to the gravity anomaly profile

The range of values of the depth to the base plane of model is considered to be from 20 m to 40 m and the spacing of h values is assumed to be 2 m. Then the standard deviation of the top depth estimates related to the different lengths of the moving average windows for each value of the depth to the base is computed. The estimated depths to the top and also their average values and standard deviations are given in tables 1 and 2.

The estimated parameters (z=10 m and h=30 m) from the free noise gravity data are alike the initial assumption, where the standard deviation of the depths to the top is zero. The minimum standard deviation (0.046) occurs at h = 32 m and z = 10.03 m while the synthetic gravity data have been corrupted with 5% random noise. The results show an error of 0.3% and 6.67% in the depths to the top and base of the finite vertical cylinder model, respectively. Sometime z and h are known, the amplitude coefficient (K) can be obtained from equation (3). Known amplitude coefficient (K) and the density contrast (ρ), the radius of the cylinder (R) can be specified from the relationship given in equation (1). When the data contain 5% random errors, the estimated average value of amplitude coefficient (K) is 18.86 mGal.m. The results are all close to the chosen parameters for initial theoretical model. This demonstrates the robustness and flexibility of the present method. The calculated gravity fields by estimated parameters from both gravity data sets, with and without random noise, using least squares method are shown in Fig 4.

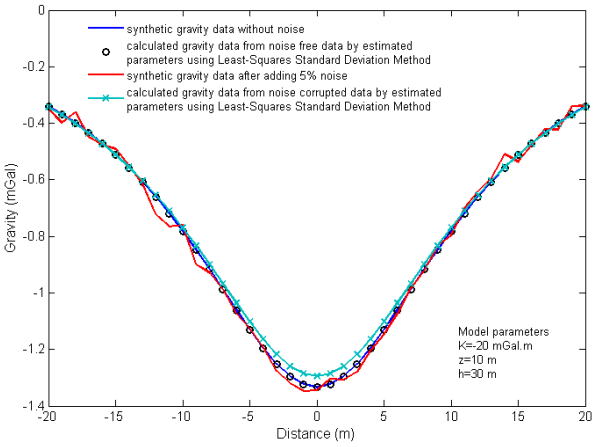

Fig 4. The observed and calculated gravity fields for the finite vertical cylinder synthetic model

3. Modular neural network

The major implication of modularity has a close relation to the notion of local computation, that is to say, each module is an independent operator and interacts with others in an integrated unit structure, in order to carry out a given duty. We apply an MNN to train and generate synthetic gravity responses. As shown in Fig 5, an MNN is a high-level neural network, consisting of a number of modules (local experts).

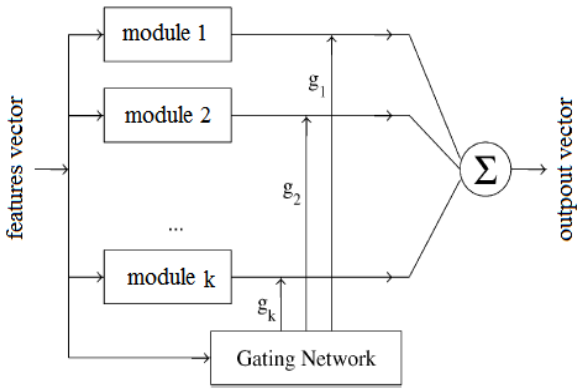

Fig 5. Sketch of the modular neural network architecture

Table 1. The moving average windows results for a finite vertical cylinder theoretical example where the parameters are: z = 10 m, h = 30 m and K = -20 mGal.m.

Assumed h Value (m)	Computed depth to the top (z) (m)				Standard deviation of depths (m)	Average value of z (m)
	S=2 m	S=3 m	S=4 m	S=5 m		
20	10.31	10.25	10.19	10.12	0.081	10.22
22	10.22	10.17	10.14	10.08	0.059	10.15
24	10.18	10.14	10.1	10.03	0.064	10.11
26	10.13	10.1	10.07	10	0.056	10.08
28	10.09	10.06	10.03	10	0.039	10.05
30	10	10	10	10	0.00	10.0
32	9.95	9.98	10	10	0.024	9.98
34	9.89	9.93	9.99	10	0.052	9.95
36	9.84	9.88	9.95	10	0.071	9.92
38	9.8	9.87	9.95	9.97	0.078	9.9
40	9.76	9.82	9.89	9.95	0.083	9.86

Table 2. The moving average windows results for a finite vertical cylinder theoretical example with added 5% random noise where the parameters are: z = 10 m, h = 30 m and K = -20 mGal.m.

Assumed h Value (m)	Computed depth to the top (z) (m)				Standard deviation of depths (m)	Average value of z (m)
	S=2 m	S=3 m	S=4 m	S=5 m		
20	10.58	10.47	10.34	10.27	0.147	10.41
22	10.47	10.35	10.19	10.12	0.158	10.28
24	10.36	10.24	10.13	10.09	0.121	10.2
26	10.28	10.19	10.15	10.08	0.083	10.17
28	10.21	10.1	9.97	10.05	0.1	10.08
30	10.17	10.08	10.03	10.01	0.071	10.07
32	10.08	10.04	10.02	9.97	0.046	10.03
34	9.91	9.82	9.94	9.98	0.068	9.91
36	9.84	9.85	9.92	9.96	0.057	9.89
38	9.73	9.78	9.85	9.92	0.082	9.82
40	9.57	9.61	9.76	9.87	0.148	9.7

The final outputs of the MNN are the amplitude coefficient, top and base depths of a finite vertical cylinder produced by summing the outputs of the modules weighted by a gating network. Each module has its own input, hidden, and output layers. An MNN contains a group of modules (also called local experts) and a gating network. The gating network learns to divide a task into several parts, which is an unsupervised learning. Each module is assigned to learn one part of the task, which is a supervised learning. Therefore, the MNN combines supervised and unsupervised learning (Haykin 1994). Fig 5 shows the architecture of the MNN. Both the modules and the gating network are connected to the same input layer. The number of output nodes and modules in the gating network must be equal. The output of each module is linked to the output layer. The output vector from the corresponding modules is weighted by the output values of the gating network so the output from a module with the best performance is transferred to the output layer with slightest change while the outputs from the other modules are weighted by a number close to zero and thus have little effect on the solution. The MNN final output is the summation of the weighted output vectors (Zhang et al. 2002).

Input pattern from the training set for each module and the gating network is the same where modules and the gating network are trained simultaneously. The gating network's duty is to specifies which module produce the most exact response to the training pattern (Haykin 1994; Zhang et al. 2002). In fact, the gating network decides how the output of the modules ought to be combined to form the final output of the system and which modules should be trained with which training patterns (Al-Garni 2013). The connection weights in that module are then allowed to be updated to increase the probability that the module will respond best to similar input patterns. For more detail, the learning algorithm has been expanded by Zhang et al. (2002).

3.1. MNN training

Training samples are a collection of input data fed to a neural network to adjust the internal network parameters along with the corresponding desired output data. Finding the internal parameters is, by itself, an inverse problem where the observations are the desired output data and the unknowns are the internal parameters. The number of training samples should be sufficient to reach the desired training accuracy (Zhang et al. 2002). Modules can be trained in parallel which reduces training times substantially and additional can be added without the need to retrain the others.

To recognize the gravity anomaly pattern by the neural network, some of its characteristic factors are defined. These factors are related to model geometry. The Fig 2 show the 2D gravity anomaly of a finite vertical cylinder model with the top and base surfaces depth of

25 m and 60 m, respectively and the amplitude coefficient of -5.5 mGal.m. The features are defined as following (Fig 6):
F1=maximum gravity, (*G*(max)).
F2= the width of the curve at points of 80% of maximum observation gravity, (W80).
F3=the gravity value at points of 80% of maximum observation gravity, (G80).
F4= the width of the curve at points of 60% of maximum observation gravity, (W60).
F5=the gravity value at points of 60% of maximum observation gravity, (G60).
F6= the width of the curve at points of 40% of maximum observation gravity, (W40).
F7=the gravity value at points of 40% of maximum observation gravity, (G40).

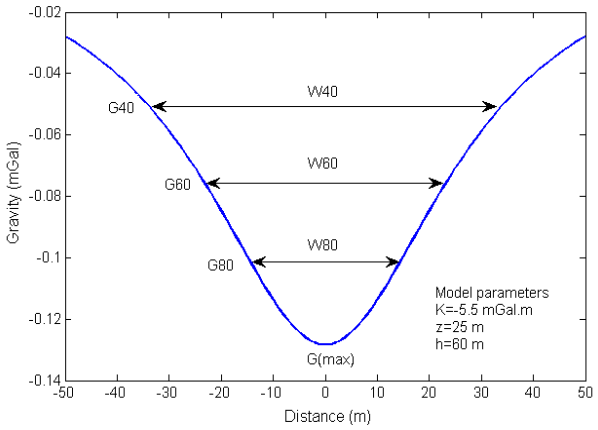

Fig 6. A pattern for estimating features from the curve of the gravity anomaly variations related to a finite vertical cylinder model

Therefore, the inputs of neural network are parameters of synthetic profile that are generated by forward modeling. Outputs are the geometric parameters of a model, namely the top and bottom depths and amplitude coefficient parameters. To generate training vectors, forward modeling is performed over 100 m profile with two-m interval. We have considered the ranges from 15 to 30 m, with 12 points for *z* parameter (the depth of the top surface), the ranges from 48 to 68 m with 18 points for *h* parameter (the depth of the base surface) and the ranges from 5 to 9 mGal.m with 10 points for the amplitude coefficient (*K*) parameter. The parameters are selected in aforementioned ranges disorderly. The choice of the expected range of the parameters depend on the behavior of measured field data and the geological information from the area under consideration.
We employ the MNN to invert the gravity data using 7 neurons for the input layer (7 features) and twenty number of nodes was also used in the hidden layer. The sigmoid transfer function was used to modify activations in the hidden layer. The number of hidden neurons can be defined more exactly by trial-and-error methods in the calculated limits. Here, the best results, obtained by trial-and-error when the number of hidden neurons is 20. Three local experts (modules) have been used for the MNN. We have computed 2160 training models (vectors) covering the ranges of the parameters. During the learning process, the learning error for each parameter can be tested individually as well as the overall root mean square. If the learning error is accepted, then we compare the misfit between the computed gravity field from the NN inversion with the observed gravity field data. If the misfit is acceptable, then the choice of the ranges is suitable. After correct training of the network, by entering parameters of anomaly profile into MNN, geometric parameters of the model are obtained.

3.2. MNN inversion for synthetic model

It is assumed that the finite vertical cylinder model to have parameters *z*=20 m, *h*=50 m and *K*=-8 mGal.m. The extracted features from the gravity anomaly profile as input vector is given to the trained MNN. The synthetic gravity anomaly and generating response from MNN inversion are shown in Fig 7. In order to investigate the effect of error on the MNN performance, a random noise of 10% added to the gravity anomaly (Fig 8). The generated gravity response from the estimated parameters using MNN inversion is shown in Fig 8. The inverted parameters by MNN are summarized in Table 3. The computed parameters are nearly equal to the initial supposed parameters. This indicates the efficiency of the MNN in inverse modeling.

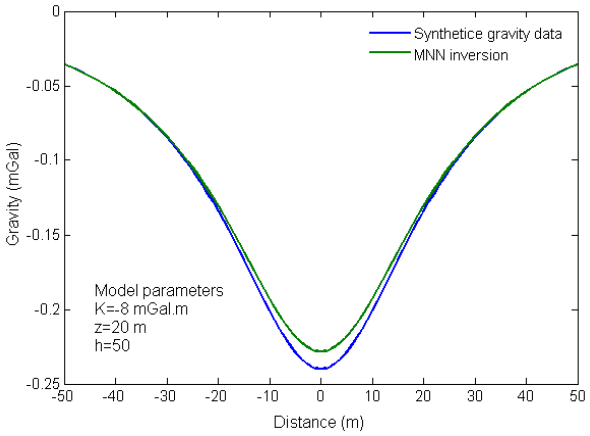

Fig 7. The synthetic gravity anomaly and generating response from MNN inversion

Table 3. Estimated parameters using MNN from the synthetic gravity anomaly

Parameter	Initial value	Estimated value from free noise data	Estimated value from noise corrupted data
K (mGal.m)	-8	-7.94	-7.78
z (m)	20	20.7	18.7
h (m)	50	51.1	52.6

4. Field example

The explained methods are employed to interpret two gravity field anomalies from the Iran and USA.

4.1. Aji-chay salt dome

The region under study is situated in the northwest of Iran. Miocene units in this region include sequences of Marl, Salt and Chalk (Fig 9).

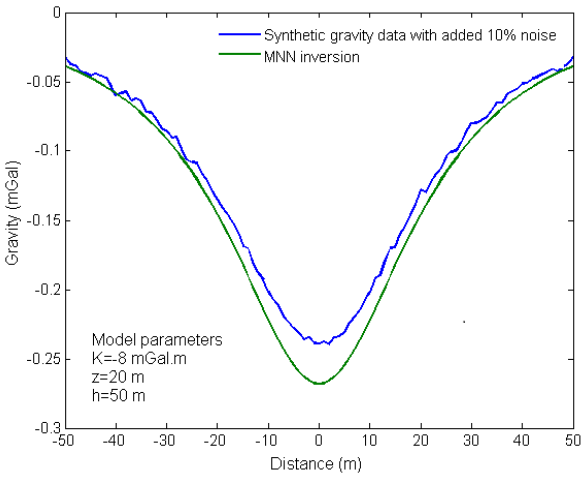

Fig 8. The synthetic gravity anomaly which contain 10% random noise and generating response from MNN inversion

The salt domes in this area are the result of the upward movement of the Neogene evaporative materials. The depth of these salt domes is low and have mostly high alloy of Potash. The main salt dome in the region under consideration is Aji-chay salt dome. The part of the gravity sampling has been determined with a white rectangular on Fig 9. Fig 10 shows the computed Bouguer gravity anomaly after making the necessary corrections and the points of the gravity reading along 10 profiles. After removing a trend (degree 2) from the Bouguer anomalies, the residual (local) gravity anomalies were computed (Fig 11). The salt dome with negative anomaly is recognizable on the residual gravity anomalies map. Profile *A* in anomaly is specified in N-S direction, which is shown in Fig 11. The defined features are specified from the observed anomaly of the profile *A* cross-section. The trained MNN is fed by the features vector. The evaluated top depth (*z*), bottom depth (*h*) and amplitude coefficient (*K*) parameters from MNN are 24.5 m, 63.8 m and -6.45 mGal.m, respectively. The obtained parameters from MNN inversion is given in Table 4.

Table 4. The estimated parameters from MNN inversion

Parameter	K (mGal.m)	h (m)	z (m)	R (m)	SE (mGal)
Estimated value	-6.45	63.8	25.4	22.6	0.0189

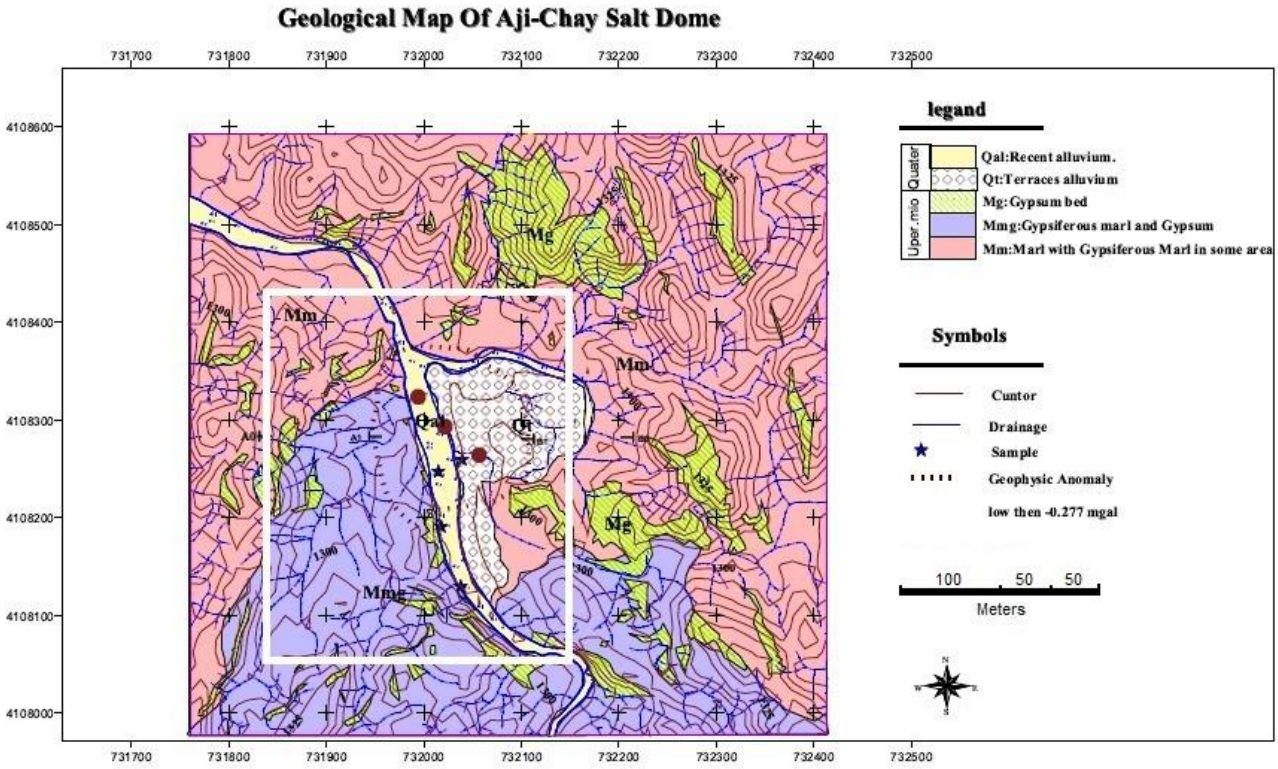

Fig 9. The geological map of the region under study

Four successive moving average windows (s=11, 12, 13 and 14 m) are used to observed gravity data related to profile A passing over Aji chay salt dome (Fig 12). The moving average residual anomalies are used to determine the depth to the top for each h value of the depth to the base using equation (6). The range of h values was chosen from 56 m to 72 m with a distance of 1 m. The depths to the top, their average values and standard deviation are given in Table 5.

Table 5. The moving average windows results for the observed gravity anomaly of the profile A cross section

Assumed h Value (m)	Computed depth to the top (z) (m)				Standard deviation of depths (m)	Average value of z (m)
	S=11 m	S=12 m	S=13 m	S=14 m		
56	33.62	27.31	22.54	18.45	6.52	25.48
58	25.74	19.55	17.28	14.81	4.68	19.35
60	28.39	18.37	20.16	16.35	5.28	20.82
62	26.35	22.5	19.83	17.73	3.72	21.6
64	25.87	24.72	22.46	20.67	2.32	23.43
66	24.3	19.06	17.74	16.36	3.47	19.37
68	22.64	16.4	14.92	15.28	3.61	17.31
70	14.83	23.76	18.57	16.44	3.89	18.4
72	22.64	18.82	28.36	21.52	4.02	22.84

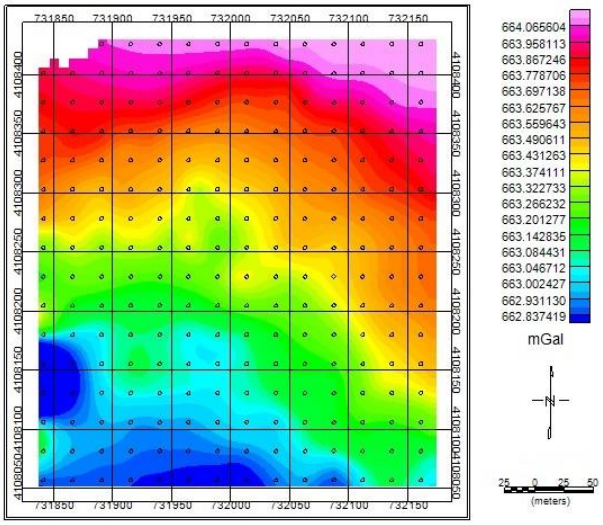

Fig 10. The Bouguer gravity anomalies map

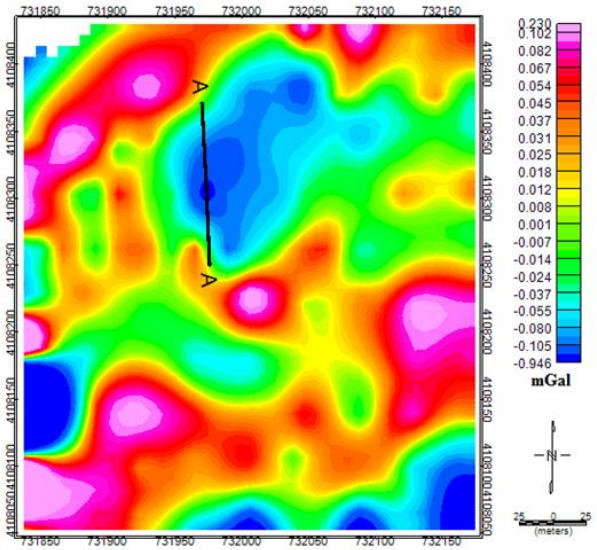

Fig 11. The residual gravity anomalies map

Table 6.The estimated parameters from least-squares standard deviation method

Parameter	K (mGal.m)	h (m)	z (m)	R (m)	SE (mGal)
Estimated value	-6.12	64	23.43	22.04	0.0195

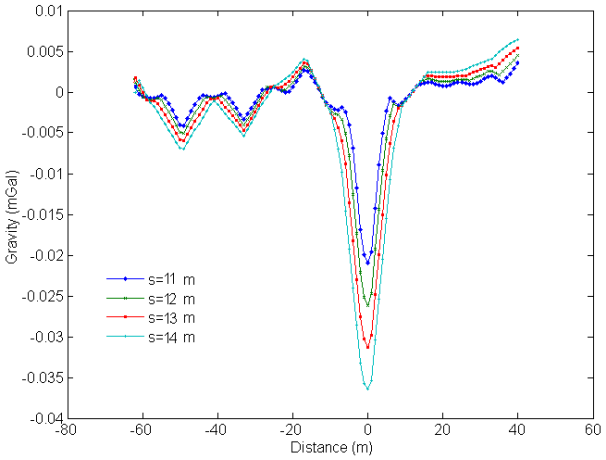

Fig 12. Moving average residual gravity anomalies of the profile A cross section for *s* = 11, 12, 13 and 14 m.

Table 5 shows that the standard deviation in the case of h = 64 m is (sd=2.32) less than the standard deviation in other cases of h values. The average value of the depth to top at h = 64 m is z = 23.43 m. The estimated average value of amplitude coefficient (K) is -6.12 mGal.m. The estimated parameters from the least-squares standard deviation method is shown in Table 6. This result is in good agreement with the MNN outputs. Fig 13 display the computed gravity responses from the estimated parameters using both methods. We have applied the standard error (SE) as the criteria in order to compare the observed and evaluated values (Asfahani and Tlas 2008),

$$SE = \sqrt{\frac{\sum_{i=1}^{N}[g_o(x_i) - g_c(x_i)]^2}{N}} \quad (7)$$

where g_o and g_c (i = 1, ..., N) are the observed and the evaluated values at the points x_i (i = 1, ..., N), respectively. The standard error for MNN and least-squares standard deviation methods are 0.0189 and 0.0195 mGal, respectively (Tables 4 and 6). As regards the estimated parameters by both methods are approximately equal, according to computed SE, the inverted parameters from MNN are closer to reality.

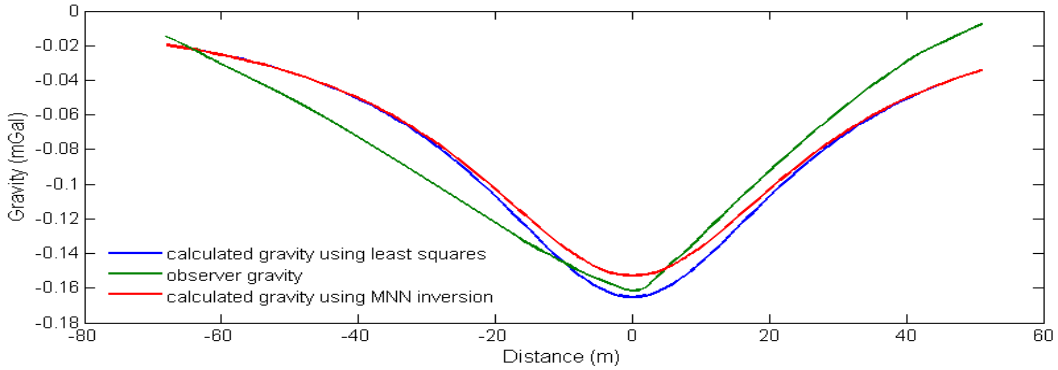

Fig 13. The observed gravity anomaly due to Aji-chay salt dome (green curve), gravity responses from MNN inversion (red curve) and gravity responses from least-squares standard deviation method (blue curve)

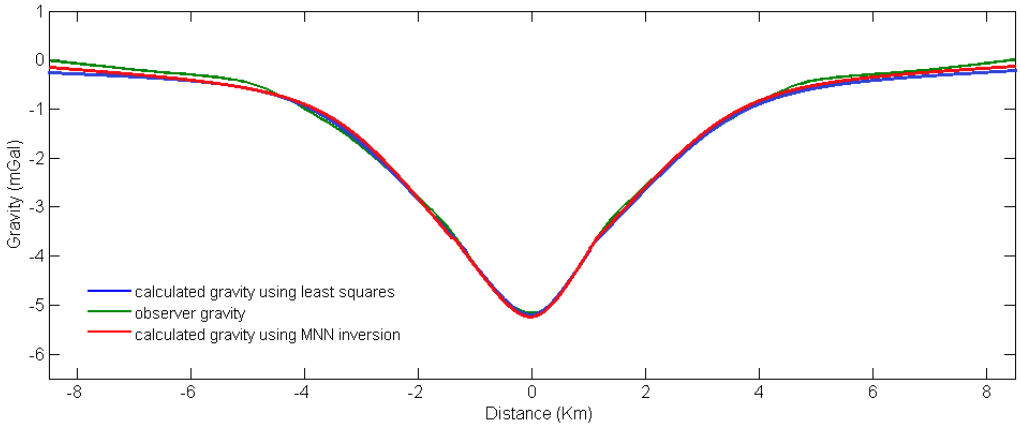

Fig 14. The observed gravity anomaly due to Louisiana salt dome (green curve), gravity responses from MNN inversion (red curve) and gravity responses from least-squares standard deviation method (blue curve)

4.2. Louisiana Salt Dome Anomaly

The second field example is a residual gravity anomaly profile passing over the center of the gravity map offshore Louisiana salt dome situated in USA (Fig 14). This anomaly has been analyzed using the least-squares standard deviation method by Abdelrahman and Abo-Ezz (2008). The average value of the depth to top at h = 9.287 km is z = 1.433 km, where the standard deviation in the case of h = 9.287 km is less than the standard deviation in other cases of h values. The estimated average value of amplitude coefficient (A) is -10.269 mGal. This suggests that the salt body is buried at z = 1.433 km and h = 9.287 km. The estimated parameters are shown in table 7. The generated gravity effect due to the estimated parameters is shown in Fig 14.

To compare, we apply the proposed method based on MNN for this gravity anomaly. The defined features are determined from the observed gravity anomaly profile. The trained MNN is fed by the features vector. The inferred top depth (z), bottom depth (h) and amplitude coefficient (K) parameters from MNN are 1.451 m, 9.263 m and -10.327 mGal.m, respectively. The obtained parameters from MNN inversion is given in Table 7. The gravity response caused by the inverted parameters is displayed in Fig 14.

We have calculated the standard error (SE) between the real gravity and the computed gravity anomalies where the estimated SE values for the least-squares standard deviation method and modular neural network inversion are given as 0.154 mGal and 0.143 mGal, respectively. This anomaly was also investigated by several authors, such as Roy et al. (2000) which introduced a new concept in Euler deconvolution method to estimate the depth of the causative mass. Furthermore, the depth obtained by Mehanee (2014) using flair function minimization is 2899 m and Biswas (2015) proposed using very fast simulated annealing global optimization for interpreting the gravity anomaly. The acquired solutions by the various method have been tabulated in Table 7. As several wells were drilled over this dome, detailed information is available (Nettleton 1976). The top of the dome was encountered in the shallowest well

at 1.2 km Up to a depth of around 1.8 km. Thus, the depth to top estimated by the least-squares standard deviation method (Abdelrahman and Abo-Ezz 2008) and presented method based on MNN are closer to the reality, where the MNN method show the smaller standard error than the least-squares standard deviation method.

Table 7. The obtained parameters from the analysis of the Louisiana salt dome gravity data using various method

Parameter		K (mGal.km)	h (km)	z (km)	SE (mGal)
Estimated values	Roy et al. (2000)	-	11.3	2.26	-
	Abdelrahman and Abo-Ezz (2008)	-10.269	9.287	1.433	0.154
	Mehanee (2014)	-16.4	-	2.899	-
	Biswas (2015)	-16.02	-	2.702	-
	MNN method	-10.327	9.263	1.451	0.143

5. Conclusions

In this study, two different methods, namely modular neural network (MNN) and least-squares standard deviation approaches were used for modeling buried structure where its geometrical shape is finite vertical cylinder. The outputs of the both methods are the top and bottom surface depths and amplitude coefficient. When the density contrast of the region under evaluation be known, the radius of a finite vertical cylinder can compute by the amplitude coefficient value. We have investigated the performance and stability both methods using the synthetic models, with and without random noise, where satisfactory results were obtained. We have applied both methods to estimate the salt dome parameters from Iran and simulate its gravity response. The resulted parameters and naturally generated gravity responses of these methods are very similar. Hence, the standard error was employed to determine which gravity response is closer to the observed gravity anomaly. The computed standard error for the modular neural network and least-squares standard deviation approaches are 0.0189 and 0.0195 mGal, respectively. Thus, the simulated gravity response from MNN inversion has better agreement with the real gravity anomaly of profile A cross section than the simulated gravity response from least square method. Based on the results obtained from MNN inversion the the depth of the Salt dome with a radius of 22.6 m, starts from 25.4 m and goes down to about 63.8 m.

For further investigation, we evaluated a gravity profile due to the Louisiana salt dome using described MNN method and compared the inverted parameters with those obtained by other method, as can be found that the inverted parameters by the both offered approaches show the better precision than other methods. The drilling information indicate a depth to top of 1.2 km to 1.8 km for the Louisiana salt dome. The estimated amounts for the depth to top by the various method are different, but the suggested methods in this study could determine the correct depth to top. The depth to top values given by the modular neural network and least-squares standard deviation approaches are 1.451 km and 1.433 km, respectively. The smaller computed standard error for the MNN method than the least-squares standard deviation approach denote the better efficiency and performance the modular neural network technique.

References

Abdelrahman EM, El-Araby TM (1996) Shape and depth solutions from moving average residual gravity anomalies. *Applied Geophysics* 36:89-95.

Abdelrahman EM, El-Araby TM, El-Araby HM, Abo-Ezz ER (2001) A new method for shape and depth determinations from gravity data. *Geophysics* 66:1774-1780.

Abdelrahman EM, Abo-Ezz ER, Essa KS, El-Araby TM, Soliman KS (2006) A Least-squares variance analysis method for shape and depth estimation from gravity data. *Journal of Geophysics and Engineering* 3:143-153.

Abdelrahman EM, Abo-Ezz ER (2008) A Least-Squares Standard Deviation Method to Interpret Gravity Data due to Finite Vertical Cylinders and Sheets. *Pure and Applied Geophysics* 165:947–965.

Abedi M, Afshar A, Ardestani VE, Norouzi GH, Lucas C (2009) Application of Various Methods for 2D Inverse Modeling of Residual Gravity Anomalies. *Acta Geophysica* 58(2):317-336.

Albora AM, Ucan ON, Özmen A, Ozkan T (2001a) Separation of Bouquer anomaly map using cellular neural network. *Journal of Applied Geophysics* 46:129-142.

Albora AM, Özmen A, Ucan ON (2001b) Residual separation of magnetic fields using a cellular neural network approach. *Pure and Applied Geophysics* 158:9-10.

Al-Garni MA (2013) Inversion of residual gravity anomalies using neural network. *Arabian Journal of Geosciences* 6:1509-1516.

Asfahani J, Tlas M (2008) An automatic method of direct interpretation of residual gravity anomaly profiles due to spheres and cylinders. *Pure and Applied Geophysics* 165(5): 981-994.

Bichsel M (2005) Image processing with optimum neural networks. *IEEE International Conference on Artificial Neural Networks, 513, IEEE*, London, 374-377.

Biswas A (2015) Interpretation of residual gravity anomaly caused by simple shaped bodies using very fast simulated annealing global optimization, *Geoscience Frontiers* 6:875-893

BotezatuIM, Visarion F, Scutu G, Cucu G (1971) Approximation of the gravitational attraction of

geological bodies. *Geophysical Prospecting* 19(2):218-227.

Cordell L, Henderson RG (1968) Iterative three-dimensional solution of gravity anomaly data using a digital computer. *Geophysics* 33:596-601.

Chua LO, Yang L (1988) Cellular neural networks: Theory. IEEE Trans. *Circuits Systems* 35(10):1257-1272.

Eshaghzadeh A, Kalantari RA (2015) Anticlinal Structure Modeling with Feed Forward Neural Networks for Residual Gravity Anomaly Profile. *8th congress of the Balkan Geophysical Society*, European Association of Geoscientists and Engineers.

Eshaghzadeh A, Hajian AR (2018) 2D inverse modeling of residual gravity anomalies from Simple geometric shapes using Modular Feed-forward Neural Network, *Annals of Geophysics 61(1):1-9.*

Eslam E, Salem A, Ushijima K (2001) Detection of cavities and tunnels from gravity data using a neural network. *Explor. Geophysics* 32:204-208.

Essa KS (2007) Gravity data interpretation using the S-curves method. *Journal of Geophysics and Engineering* 4:204–213.

Hajian AR (2004) Depth estimation of gravity data by neural network. M. Sc. thesis, *Tehran University*, Iran (In Persian).

Hammer S (1974) Approximation in gravity interpretation calculation. *Geophysics* 39: 205–222.

Haykin S (1994) Neural networks: a comprehensive foundation. *Macmillan*, New York.

Masket AVH, Macklin R, Schmitt HWG (1956) Tables of Solid Angles and Activations: 1. Solid Angle Subtended by a Circular disc; 2. Solid Angle Subtended by a Cylinder; 3. Activation of a Cylinder by a Point Source, *ORNL-2170, Unclassif. Tech. Inf. Serv. Extens.*, Oak Ridge, Tenn.

Mehanee SA (2014) Accurate and efficient regularised inversion approach for the interpretation of isolated gravity anomalies. *Pure and Applied Geophysics* 171: 1897-1937.

Nettleton LL (1976) Gravity and Magnetics in Oil Prospecting. *McGraw-Hill Book Co*.

Osman O, Muhittin AA, Ucan ON (2006) A new approach for residual gravity anomaly profile interpretations: Forced Neural Network (FNN), *Annals of Geophysics* 49(6).

Osman O, Muhittin AA, Ucan ON (2007) Forward modeling with Forced Neural Networks for gravity anomaly profile, *Mathematical Geology* 39:593-605.

Pick M, Picha J, Vyskosil V (1973) Theory of the Earth's Gravity Field. (Academic publishing house of the Czechoslovakia), *Academy of Sciences*, Prague.

Roy L, Agarwal BNP, Shaw RK (2000) A new concept in Euler deconvolution of isolated gravity anomalies, *Geophysical Prospecting* 48:559-575.

Salem A, Ravat D, Johnson R, Ushijima K (2001) Detection of buried steel drums from magnetic anomaly data using a supervised neural network, *Journal of Environmental and Engineering Geophysics* 6:115-122.

Skeels DC (1963) An approximate solution of the problem of maximum depth in gravity interpretation, *Geophysics* 28:724-735.

Talwani M, Ewing M (1960) Rapid computation of gravitational attraction of three-dimensional bodies of arbitrary shape, *Geophysics* 25:203-225.

Tanner JG (1967) An automated method of gravity interpretation, *Geophysical Journal International* 13:339-347.

Zhang L, Poulton MM, Wang T (2002) Borehole electrical resistivity modeling using neural networks, *Geophysics* 67:1790-1797.